Computer Simulation of Crystallization Kinetics in Fiber-Reinforced Composites

TH. KRAUSE, G. KALINKA, C. AUER, and G. HINRICHSEN*

Technical University of Berlin, Institute of Nonmetallic Materials, Polymer Physics, Englische Str. 20, D-10587 Berlin 12, Germany

SYNOPSIS

A computer simulation model was developed to investigate spherulitic growth in polymers of infinite and plate-limited volume as well as in fibre-reinforced polymer composite systems. Parameters like thermal nucleation rate and athermal nucleation density, plate distance, and fibre content were varied. The simulation crystallization process was evaluated following Avrami's method in the case of infinite volume and by stepwise approximation by Avrami functions in the case of limited volume. In addition, the simulation method allows the visualization of the growing entities at any phase of crystallization. Therefore the geometry of growing entities can be easily compared with the corresponding crystallization exponent. A good agreement between the crystallization exponent and the growth geometry was found.

Depending on nucleation mode, "infinite" systems yield Avrami exponents of 3 and 4. In plate-limited volume, a transcrystallization effect was observed in case of high athermal nucleation density on plate surface and large plate distances. This particular skin effect decreases the three-dimensional growth to a one-dimensional needle-shaped one. Small plate distance changes the spherical to a disk-like growth, resulting in crystallization exponents of 2 or 3, depending on nucleation mode. The crystallization behaviour of fibre-reinforced composite systems is more complex. Low fibre content or large fibre distance and high athermal nucleation density on the fibre surface induce the formation of transcrystalline zones. The three-dimensional growth of the spheres at the beginning is restricted by their neighbours, so that their geometry changes to a pyramidical one. They grow with a front normal to the fibre surface and the crystallization exponent is shifted in between 2.0 and 2.6 depending on nucleation density. High fibre content leads to a growth along the triangular channels between three adjacent fibres; the corresponding exponent amounts to 1.6. © 1994 John Wiley & Sons, Inc.

INTRODUCTION

The properties of thermoplastic fibre-reinforced composites are significantly influenced by the morphology of the polymer matrix. Effects like transcrystallization change mechanical properties due to a preferred orientation of crystal growth. The morphology is determined by the nucleation rate on fibre surface, fibre distance, and growth velocity of the spherulites. The relations between these parameters and the resulting morphology of highly filled composites are widely unknown. Direct studies of the crystallization process in highly filled composites, especially by optical methods, are difficult to carry out. Therefore, an indirect method, differential scanning calorimetry (DSC), is often used to monitor the crystallization process by its exothermic heat flow. In many cases, it has been observed that the crystallization exotherms of crystallizing composite materials lead to nonlinear trajectories in the Avrami plots. The interpretation of this effect, however, is quite difficult. For this reason, it was desirable to investigate the crystallization of an idealized model system that allows the exact definition of all basic parameters. Special attention was drawn to implement a correct model for a system of unlimited

* To whom correspondence should be addressed.

Journal of Applied Polymer Science, Vol. 51, 399–406 (1994)
 CCC 0021-8995/94/030399-08

and plate-limited volume before investigating a fibre-filled composite system.

The mathematical problem of filling an infinite volume or plane by randomly distributed growing elements was first solved by Poisson.[1] Evans,[2] Avrami,[3] and Kolmogoroff[4] adapt the Poisson function in order to describe crystallization kinetics. The time-dependent formulation of the crystallizing portion of a polymer at constant temperature T, $X(t)$, is well known in the form of the so-called Avrami equation,

$$X(t) = 1 - e^{-kt^n} \quad (1)$$

where k is a constant, depending on nucleation rate and growth velocity, and n is an exponent describing the growth order. Of interest in our investigation is that this quantity varies with the mode of nucleation and with the geometry of growing entities. Polymers usually crystallize in the form of so-called spherulites. Athermal nucleation and spherulitic growth lead to an Avrami exponent of 3, thermal nucleation and spherulitic growth to a value of 4.[5]

However, these values were never found with existing polymers due to the differences between the mathematical model and real properties of the material.[6] Three possible reasons for this difference can be assumed: First, the nucleation mode is a mixture of thermal and athermal nucleation, resulting in exponents between 3 and 4.[7] Second, the spherulites are not compact spheres with a well-defined growth front. The crystallization does not take place only at the growth front, but also inside the spherulites in dependence on time. This effect shifts the crystallization exotherm to longer time and to lower exponents. The third reason may result from a limitation of the crystallizable volume by incorporation of filler materials like spheres, fibres, or plates. In highly filled systems, the original three-dimensional geometry of spherulites can be reduced to two-dimensional discs or one-dimensional needles. A lower value of growth order leads to a lower exponent in the Avrami equation.

All these effects influence the basic assumptions for describing the crystallization process as a simple Avrami process. However, knowing about the real circumstances of polymeric crystallization, an Avrami plot is usually applied to describe the crystallization kinetics.

In recent years, some computer simulations of crystallization kinetics in spherulitic systems have already been done. Hay and Przekop[8] investigated the crystallization process in simulated systems of growing spheres, discs, and rods. Their model consists of a three-dimensional cube, containing randomly distributed start-points of growing entities and a lattice of observation points gridding the whole system. The observation points represent small volume elements. All spheres start growing simultaneously and simulate an athermal nucleation. The time-dependent crystallized portion of the system was defined by the ratio of the nonoverlapped to the total number of observation points in dependence on sphere diameter. Approximately 200 spheres and 150 observation points were used for the calculation. The authors obtained Avrami exponent values from 2.90 to 2.95. However, the ideal value of 3.0 could not be reached. One reason for this result may be that the influence of system boundaries was not completely excluded. To simulate an "infinite" volume, the probability for reaching a crystallizing volume element inside the bulk volume has to be identical for any direction and position. Therefore, the elimination of observation points near the system boundaries with less probability is absolutely necessary.

Galeski and Piórkowska[9-11] studied spherulites pattern and size distribution using a similar simulation model in order to confirm their analytical calculations. They achieved a good agreement between computed and theoretical values of Avrami exponents. Lambrigger et al.[12] did some work on the incubation time of nucleation by a simulation.

A new theoretical approach of the crystallization in thin polymer films was developed by Billon et al.[13] They used a net of observation points placed inside a parallelepiped, the length and width of which was much greater than its thickness. Nuclei were placed both inside the volume and on the surface. The transformed volume fraction of the whole system was defined by the number of observation points reached by the growing spherulites at a given time in relation to the total number of observation points. In thin films, a significant lowering of the crystallized portion was found, but no specified values of Avrami exponents were reported.

EXPERIMENTAL

Our newly developed model contains various components: growing spheres, fillers, external boundaries, and the inner observation volume (Fig. 1). The growing spheres are described by their positions, activation times, and growth velocities. All randomly positioned startpoints are located inside the external boundaries, but outside the fillers' space. Thermal nucleation is simulated by placing start-points (nu-

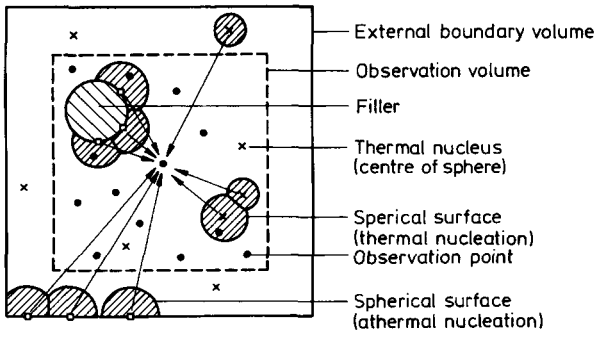

Figure 1 Sectional view of our three-dimensional simulation model. Infinite volume simulation including one filler.

clei) in the bulk and each start-point is described by a different activation time in dependence on the given nucleation rate G. Athermal nucleation is realized by placing a given number of start-points correlating to the nucleation density D (in particular on the fillers' or on the external boundary surface) and by assigning the same activation time to each nucleus. After positioning the start-points, the nuclei grow with constant growth velocity v.

A new and important feature of our model is the possibility of insulating the observation area from the system boundaries so that the crystallization kinetics within an infinite volume can be calculated.

The evaluation procedure starts after fixing the geometry of the external boundaries, the inner observation volume, the fillers, and the start-points as described above. Then, an observation point is randomly positioned anywhere inside the observation area, but outside the fillers. For each sphere (coordinates X_S, Y_S, Z_S), the time $t_{p,s}$ for reaching this

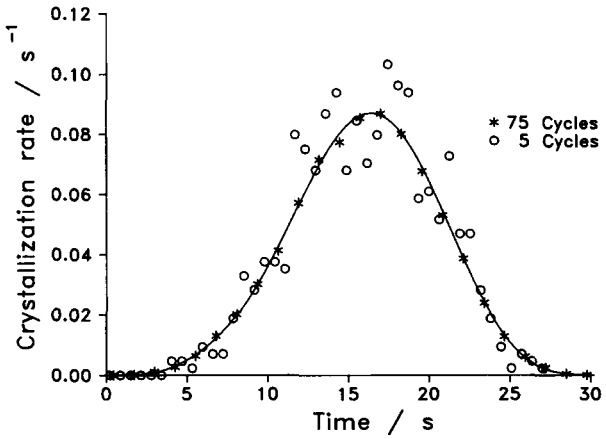

Figure 2 Crystallization rate as a function of time. Improvement by increasing calculation cycles.

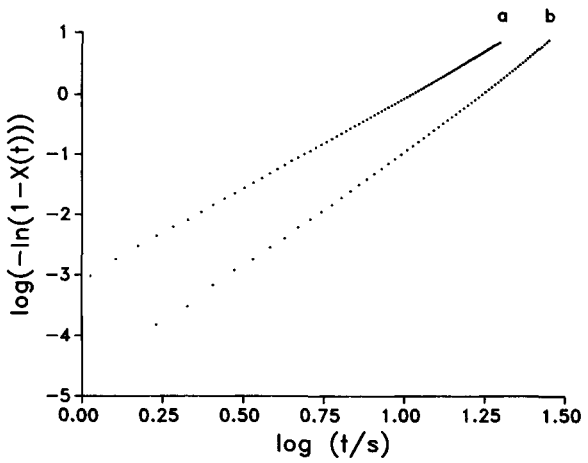

Figure 3 Avrami plots for infinite volume. (a) Athermal nucleation density $D = 200\ \mathrm{mm}^{-3}$, $v = 10\ \mu\mathrm{m\ s}^{-1}$, $\bar{n} = 3.0$, $\log k = -3.1$. (b) Thermal nucleation rate $G = 10\ \mathrm{mm}^{-3}\ \mathrm{s}^{-1}$, $v = 10\ \mu\mathrm{m\ s}^{-1}$, $\bar{n} = 4.0$, $\log k = -4.9$.

observation point (coordinates X_p, Y_p, Z_p) is calculated by the following equation:

$$t_{p,s} = t_a \cdot \frac{\sqrt{(X_p - X_s)^2 + (Y_p - Y_s)^2 + (Z_p - Z_s)^2}}{v}. \quad (2)$$

The shortest of all calculated times $t_{p,s}$ is taken as the "crystallization time" for this observation point. In an inner loop, the crystallization times for about 200 randomly positioned observation points are obtained. In an outer loop, new start-points and start-times of spheres were randomly fixed in order to evaluate another system with identical simulation parameters, passed through 75 times. All of the about 15.000 collected crystallization times are classified by time intervals, resulting in a distribution of crystallization rate as a function of time (Fig. 2). This distribution contains the same information as the heat flow-time traces of DSC scans, because the exothermic heat flow of an isothermal crystallization process is directly proportional to the crystallization

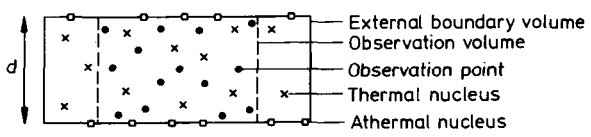

Figure 4 Sectional model view of nuclei distribution and observation volume in plate-limited systems. Thermal nucleation only in the bulk (system one) and athermal nucleation only on the plate surface (system two).

rate. Step by step integration leads to the time-dependent degree of crystallization. Both Avrami exponent n and constant k can be obtained from the double logarithmic form of the Avrami equation:

$$\log\{-\ln[1 - x(t)]\} = \log k + n \cdot \log t. \quad (3)$$

These parameters, especially the exponent n are used to discuss the growth order of the spherulites during the crystallization process. In addition, different stages of crystallization of the simulated system can be visually controlled and photographed from the computer screen. This is an essential tool for the interpretation of the nonlinear trajectories observed in the case of crystallization under limitations in space. These plots were approximated by stepwise Avrami functions. The resulting exponents are called "crystallization exponents" to express their difference to the "pure" Avrami exponents.

RESULTS

Infinite Volume

In order to simulate the properties of an infinite volume in a correct way it is necessary to eliminate the influence of the external system boundaries. If the distance between boundaries of observation volume and the external system boundaries is large enough, the crystallization process inside the observation volume does not "see" the limitations in space (Fig. 1). This critical distance depends on nucleation density and corresponds to the average distance between the start-points. After collecting the results of enough (some 10,000) crystallization points in such an infinite system, we obtained a straight line in the Avrami plot with the theoretically proposed exponents of 3.0 for athermal and 4.0 for thermal nucleation (Fig. 3). Therefore, the computer simulation seems to reproduce the results of the Avrami theory correctly.

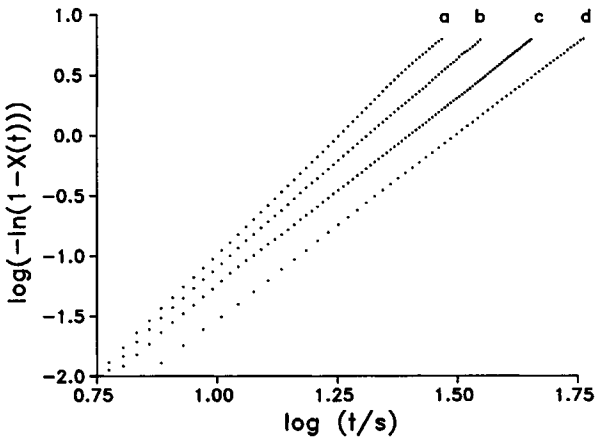

Figure 5 Avrami plots for various plate distances $d/\mu m$. Thermal nucleation only in the bulk with nucleation rate $G = 10\ mm^{-3}\ s^{-1}$, $v = 10\ \mu m\ s^{-1}$. (a) $d = 1000$, $n_1 = 4.0$, $n_2 = 3.9$, $n_3 = 3.8$, $\bar{n} = 3.9$; (b) $d = 125$, $n_1 = 4.0$, $n_2 = 3.7$, $n_3 = 3.4$, $\bar{n} = 3.5$; (c) $d = 63$, $n_1 = 3.8$, $n_2 = 3.1$, $n_3 = 3.1$, $\bar{n} = 3.2$; (d) $d = 31$, $n_1 = 3.4$, $n_2 = 3.1$, $n_3 = 3.0$, $\bar{n} = 3.1$.

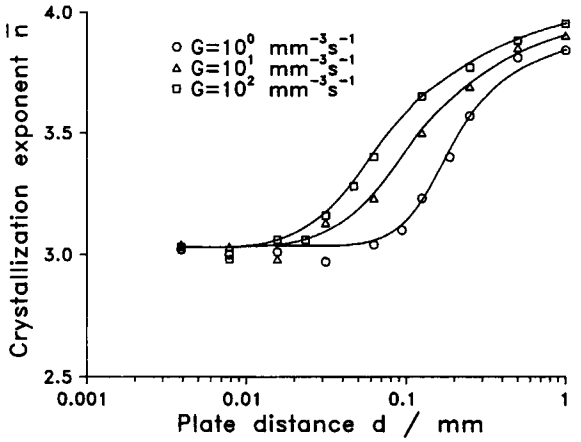

Figure 6 Average crystallization exponent $\bar{n}$ as a function of plate distance. Various thermal nucleation rates G only in the bulk.

Plate-Limited Volume

Plate-limited volumes are characterized by the identity of the boundaries of the inner observation volume and the whole system in one dimension. To simulate an infinite crystallizing polymer film, distances between observation and external volume in the two remaining dimensions have to be much larger (Fig. 4). For our investigations we used the geometry of a cube lowering its height and broadening its width in order to obtain just the same volume for each plate distance. Two types of nucleation were introduced. The first one simulates only nuclei of growing spheres in the bulk and none on the plate surface; the second one only nuclei on the plate surface and none in the bulk. Thermal nucleation was chosen in the first case and athermal in the second.

Due to the effect of limitations, the following plots are characterized by nonlinear trajectories in the double logarithmic scale. Therefore, the plots were subdivided into three parts, resulting in crystallization exponents n_1, n_2, and n_3 (early-, middle-, and late-crystallization stage) by Avrami functions

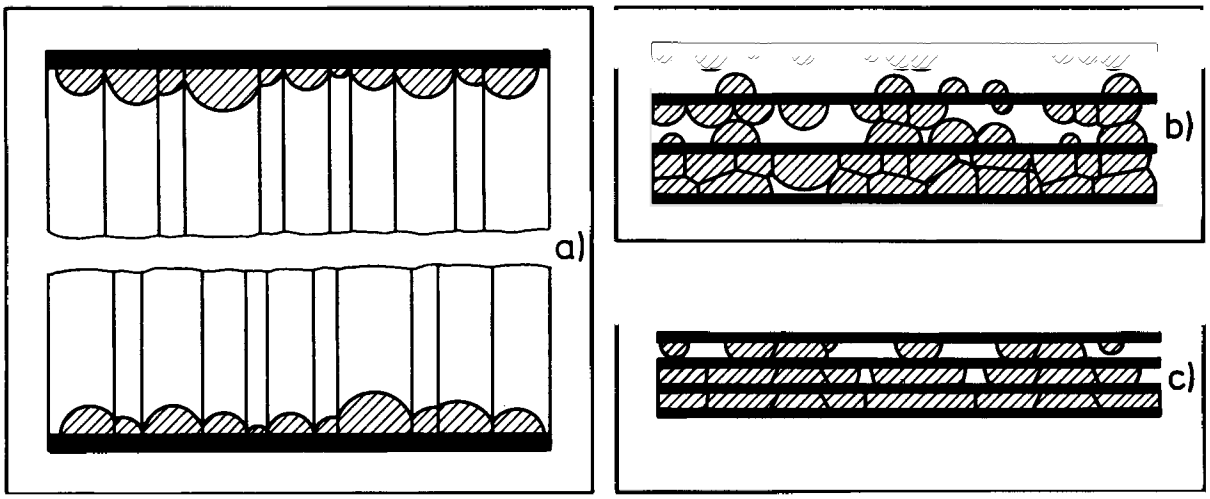

Figure 7 Simulation of growing spherulites for various crystallization times t and different plate distances d. Athermal nucleation only on the plate surface with nucleation density $D = 1000\ \text{mm}^{-2}$, $v = 10\ \mu\text{m s}^{-1}$. (a) $d = 1000\ \mu\text{m}$, $t = 4$ s, 35 s; (b) $d = 31.25\ \mu\text{m}$, $t = 1$ s, 1.5 s, 2 s, 3 s; (c) $d = 7.813\ \mu\text{m}$, $t = 1$ s, 1.5 s, 2 s, t_∞.

within these stage limits. To eliminate the problem of selecting and comparing the correct stages, the calculation of an average crystallization exponent $\bar{n}$ was also carried out to characterize the more general growth order of the complete crystallization process.

In both nucleation types, the crystallization exponent n_1 of 3 or 4, respectively, at the beginning of spherical growth was obtained. Depending on nucleation density and plate distance, the exponent decreases with increasing crystallization time. There are various reasons for this behaviour taking place within the two systems.

In the system of limited plate distance and thermal nucleation only in the bulk, growing spheres come into contact with the plates when they have a sufficiently large size. After contacting, these spheres can grow only in a restricted form resulting in lower crystallization exponents n_2, n_3 (Fig. 5). The portion of the spheres growing under this volume restriction increases with decreasing plate distance. In very thin films all entities only grow with a disc-like geometry not with spherical. Therefore, the time of three-dimensional growth becomes very short and the main part of the volume is filled by growing discs. This effect lowers the average crystallization exponent $\bar{n}$ from nearly 4 to nearly 3 (Fig. 6).

In the case of athermal nucleation on the plate surface, the circumstances are more complicated. At an early stage the spheres grow three-dimensionally (Figs. 7a, 8a–g). Depending on nucleation density, each growing sphere limits the volume of its neighbours. Therefore, they grow with a common front, each of them in a one-dimensional tube (Fig. 7a). The so-called transcrystallization results from high nucleation density and large plate distance, and as a consequence the corresponding crystallization exponent n_2 becomes nearly 1 (Fig. 8f,g), which is in good agreement with the visible one-dimensional growth. From computations of unusually high ex-

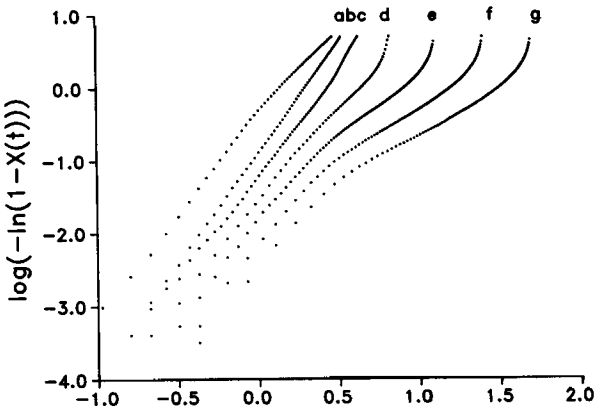

Figure 8 Avrami plots for various plate distances $d/\mu\text{m}$. Athermal nucleation only on the plate surfaces with nucleation density $D = 1000\ \text{mm}^{-2}$, $v = 10\ \mu\text{m s}^{-1}$. (a) $d = 8$, $n_1 = 2.9$, $n_2 = 2.4$, $n_3 = 2.0$, $\bar{n} = 2.5$; (b) $d = 32$, $n_1 = 3.0$, $n_2 = 3.0$, $n_3 = 3.1$, $\bar{n} = 3.0$; (c) $d = 63$, $n_1 = 2.9$, $n_2 = 2.8$, $n_3 = 3.8$, $\bar{n} = 2.9$; (d) $d = 125$, $n_1 = 2.8$, $n_2 = 2.1$, $n_3 = 6.0$, $\bar{n} = 2.6$; (e) $d = 250$, $n_1 = 2.9$, $n_2 = 1.5$, $n_3 = 5.0$, $\bar{n} = 2.1$; (f) $d = 500$, $n_1 = 2.8$, $n_2 = 1.3$, $n_3 = 4.9$, $\bar{n} = 1.8$; (g) $d = 1000$, $n_1 = 2.7$, $n_2 = 1.2$, $n_3 = 3.5$, $\bar{n} = 1.5$.

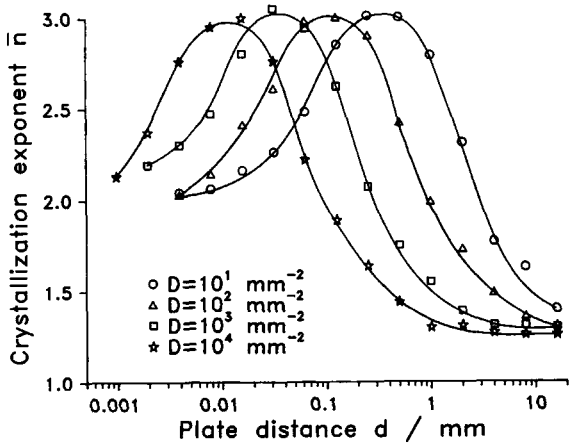

Figure 9 Average crystallization exponent $\bar{n}$ as a function of plate distance. Various athermal nucleation density D only on the plate surface.

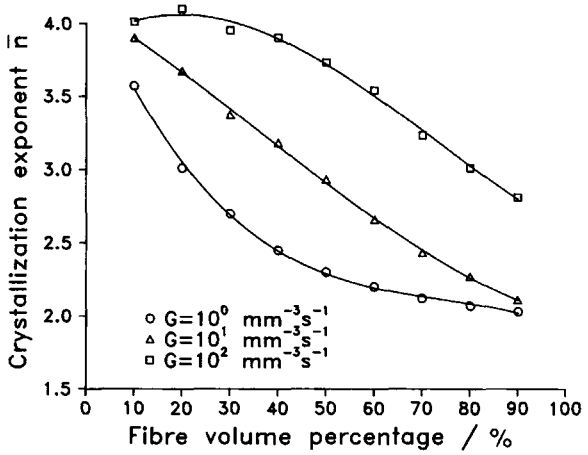

Figure 11 Average crystallization exponent $\bar{n}$ as a function of fibre volume percentage. Various thermal nucleation rate G only in the bulk.

ponents n_3 at high plate distances near the end of crystallization, it can be assumed that the sector of colliding crystallization fronts has a significant higher growing order. This process does not obey an exponential law.

If the plate distance is smaller than the average nuclei distance, the growing spheres arrive at the opposite plate before restricting the volume of their neighbours. After a three-dimensional beginning, the growth mode changes to a two-dimensional disc-shaped type (Fig. 7c). A smaller plate distance lowers the growth order of the growing spheres and shifts the corresponding crystallization exponents n_3 as well as $\bar{n}$ toward 2 (Figs. 8a, 9).

Between the one-dimensional transcrystalline and the two-dimensional disc-shaped growth geometry, a maximum of the average crystallization exponent $\bar{n}$ is reached if plate distance and average nuclei distance are in the same range (Fig. 9). Growing spheres come into contact with their neighbours in about the same time interval as they arrive at the opposite plate (Fig. 7b). Therefore, the growth geometry is mainly three-dimensional, which correlates with the resulting average crystallization exponent $\bar{n}$ of nearly 3 (Fig. 8b).

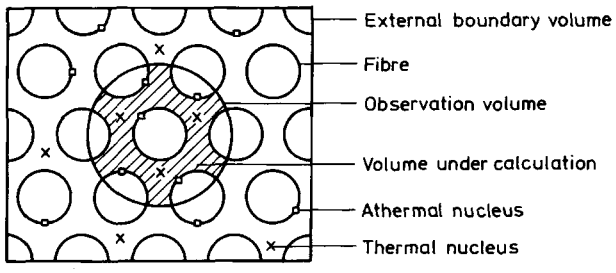

Figure 10 Sectional model view of fibre-reinforced composites. Thermal nucleation in the bulk and athermal nucleation on the fibre surface.

Fibre Reinforced Composites

In order to simulate the growth of spherulites within fibre-reinforced composites the same rules are applied as in the case of infinite volume. The model volume was great enough to ensure an inner obser-

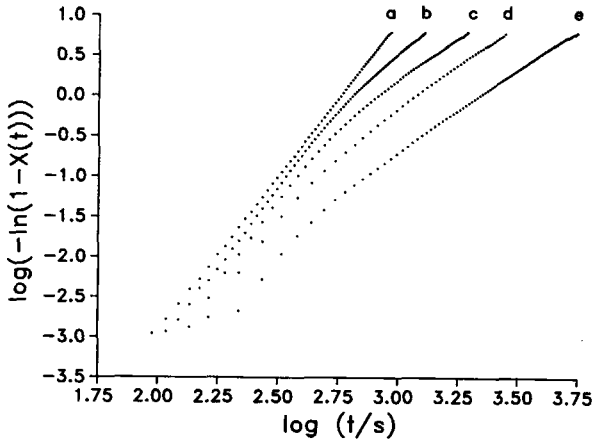

Figure 12 Avrami plots for various fibre-volume percentages $F_v/\%$. Thermal nucleation only in the bulk with nucleation rate $G = 10\ \mathrm{mm^{-3}\ s^{-1}}$, $v = 0.1\ \mu\mathrm{m\ s^{-1}}$. (a) $F_v = 10$, $n_1 = 4.0$, $n_2 = 3.9$, $n_3 = 3.9$, $\bar{n} = 3.9$; (b) $F_v = 30$, $n_1 = 3.9$, $n_2 = 3.7$, $n_3 = 2.5$, $\bar{n} = 3.4$; (c) $F_v = 50$, $n_1 = 4.1$, $n_2 = 2.9$, $n_3 = 2.1$, $\bar{n} = 2.9$; (d) $F_v = 70$, $n_1 = 4.1$, $n_2 = 2.5$, $n_3 = 2.1$, $\bar{n} = 2.4$; (e) $F_v = 90$, $n_1 = 4.1$, $n_2 = 2.3$, $n_3 = 2.0$, $\bar{n} = 2.3$.

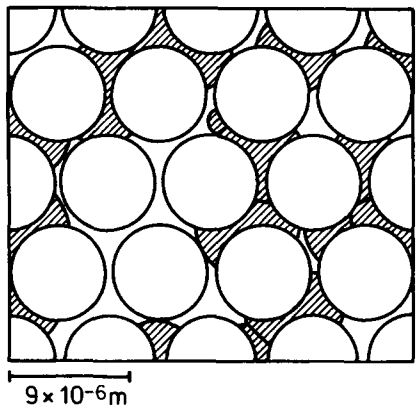

Figure 13 Simulation of growing spherulites in a highly filled fibre-reinforced system with F_v = 80%. Athermal nucleation density $D = 1*10^4$ mm^{-2} only on the fibre surface. log t = 1.6, v = 0.1 μm s^{-1}.

vation area with the properties of an infinite composite. The inner observation area consists of seven fibres arranged in a hexagonal unit cell. The complete system contains 57 fibres (Fig. 10).

Similar to the computations with the plate-limited systems, two types of composites were studied. The first one simulated nuclei only in the bulk, and the second one simulated them only on the fibre surface. Thermal nucleation was chosen in the first case and athermal in the second. Both systems lead to a three-dimensional spherical growth at the beginning of crystallization.

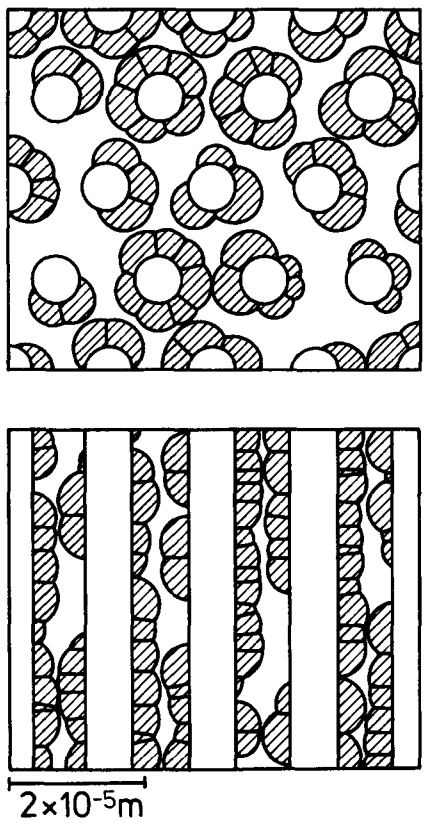

Figure 15 Simulation of growing spherulites in a low filled fibre-reinforced system with F_v = 20%. Athermal nucleation density $D = 5*10^4$ mm^{-2} only on the fibre surface. log t = 1.6, v = 0.1 μm s^{-1}. (a) Vertical fibre intersection; (b) parallel fibre intersection.

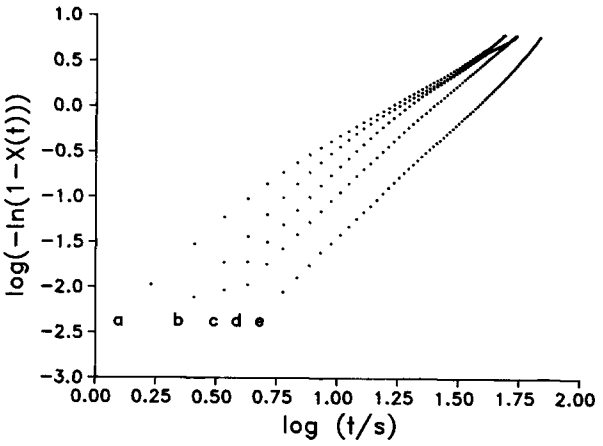

Figure 14 Avrami plots for various athermal nucleation density D/mm^{-2} only on the fibre surface. Fibre-volume percentage F_v = 80%, v = 0.1 μm s^{-1}. (a) $D = 5.0 \cdot 10^5$, n_1 = 2.7, n_2 = 1.8, n_3 = 1.6, $\bar{n}$ = 1.7; (b) $D = 1.0 \cdot 10^5$, n_1 = 2.9, n_2 = 2.0, n_3 = 1.7, $\bar{n}$ = 2.0; (c) $D = 5.0 \cdot 10^4$, n_1 = 3.0, n_2 = 2.5, n_3 = 1.7, $\bar{n}$ = 2.3; (d) $D = 2.5 \cdot 10^4$, n_1 = 3.0, n_2 = 2.6, n_3 = 2.3, $\bar{n}$ = 2.5; (e) $D = 1.0 \cdot 10^4$, n_1 = 3.0, n_2 = 2.6, n_3 = 2.8, $\bar{n}$ = 2.7.

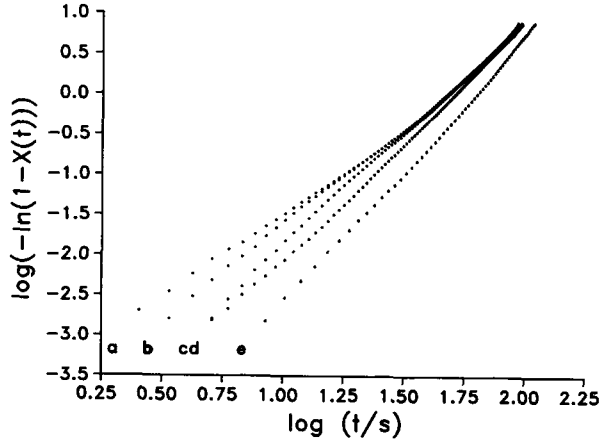

Figure 16 Avrami plots for various athermal nucleation density D/mm^{-2} only on the fibre surface. Fibre-volume percentage F_v = 20%, v = 0.1 μm s^{-1}. (a) $D = 5.0 \cdot 10^5$, n_1 = 2.3, n_2 = 2.0, n_3 = 2.9, $\bar{n}$ = 2.4; (b) $D = 1.0 \cdot 10^5$, n_1 = 3.0, n_2 = 2.3, n_3 = 2.9, $\bar{n}$ = 2.4; (c) $D = 5.0 \cdot 10^4$, n_1 = 3.0, n_2 = 2.6, n_3 = 2.9, $\bar{n}$ = 2.7; (d) $D = 2.5 \cdot 10^4$, n_1 = 2.9, n_2 = 3.1, n_3 = 3.1, $\bar{n}$ = 3.0; (e) $D = 1.0 \cdot 10^4$, n_1 = 3.2, n_2 = 3.1, n_3 = 3.5, $\bar{n}$ = 3.3.

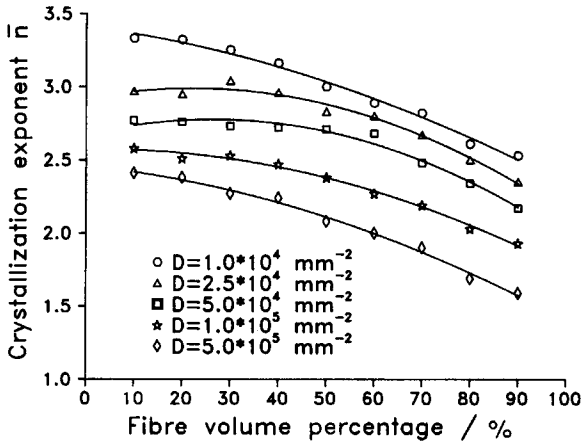

Figure 17 Average crystallization exponent $\bar{n}$ as a function of fibre-volume percentage. Various athermal nucleation density D only on the fibre surface.

Smaller fibre distances and lower nucleation density in the system with thermal nuclei in the bulk decrease the order of growth (Fig. 11). This effect is not as strong as in the plate-limited system due to the different distances between nuclei positions and the surrounding fibres. Very small fibre distances lead to a mainly one-dimensional growth in the tube between three adjacent fibres, resulting in crystallization exponents n_3 of nearly 2, which suggests a one-dimensional growth in the case of thermal nucleation (Fig. 12d,e). At greater fibre distances spheres are able to grow mainly three-dimensionally (Fig. 12a,b).

In the system with athermal nuclei only on the fibre surface, a critical range of fibre distances, depending on nucleation density on the fibre surface, can be observed. If fibre distance is less than a critical value, growing spheres arrive at the next fibre surface before restricting the growth of the neighbouring spheres (Fig. 13). At high nucleation densities, the crystallization exponent n_3 is reduced to 1.6 (Fig. 14a), which is in good agreement to the visible one- and two-dimensional growth between three adjacent fibres. On the other side, if the fibre distance is relatively large and the nucleation density on the fibre surface is sufficiently high, the spheres (not the adjacent fibres) restrict the growth process of their neighbours and a transcrystalline zone appears. The growth geometry in the transcrystalline zone is mainly pyramidical on viewing the vertical fibre intersection (Fig. 15a) and disc-shaped at the parallel one (Fig. 15b), resulting in crystallization exponents n_2 in the range of 2.0–2.6, depending on fibre surface nucleation density (Fig. 16a–c).

Under certain assumptions for the composite model, the calculations lead to unusually high crystallization exponents (Fig. 16e). In the case of low nucleation densities on the fibre surface and large fibre distances, the growing spheres include the fibres at the beginning of crystallization (imagine lower nucleation density in Fig. 15a). This surrounding process has a significant higher order than the usual three-dimensional spherical growth geometry. This observation is in a good agreement with the results of Dobbert,[14] who showed that exponents for such geometries may reach values of 4–5 in the case of athermal nucleation. Nevertheless, the average crystallization exponent $\bar{n}$ is being shifted down to lower values by higher fibre contents as well as by higher fibre nucleation densities (Fig. 17).

The authors thank the Bundesministerium für Forschung und Technologie (BMFT, project number 03M10.38A) for financial support.

REFERENCES

1. S. D. Poisson, *Recherches sur la Probabilité de Jugements en Matière Criminelle et en Matière Civile*, Bachelier, Paris, 1837.
2. U. R. Evans, *Trans. Faraday Soc.*, **41**, 365 (1945).
3. M. J. Avrami, *J. Chem. Phys.*, **7**, 1103 (1939); ibid. **8**, 212 (1940); ibid. **9**, 177 (1941).
4. A. N. Kolmogoroff, *Isvest. Akad. Nauk SSSR Ser. Math.*, **1**, 335 (1937).
5. W. Dietz, *Coll. Polym. Sci.*, **259**, 413 (1981).
6. H. G. Zachmann, *Fortschr. Hochpolym. Forsch.*, **3**, 581 (1964).
7. E. Piórkowska and A. Galeski, *J. Polym. Sci., Polym. Phys. Ed.*, **23**, 1723 (1985).
8. J. N. Hay and Z. J. Przekop, *J. Polym. Sci., Polym. Phys. Ed.*, **17**, 951 (1979).
9. A. Galeski, *J. Polym. Sci., Polym. Phys. Ed.*, **19**, 721 (1981).
10. A. Galeski and E. Piórkowska, *J. Polym. Sci., Polym. Phys. Ed.*, **19**, 731 (1981).
11. A. Galeski and E. Piórkowska, *Coll. Polym. Sci.*, **261**, 1 (1983).
12. M. Lambrigger, J. Mayer, R. M. Thomas, and I. Tomka, *Polym. Bull.*, **23**, 271 (1990).
13. N. Billon, J. M. Escleine, and J. M. Haudin, *Coll. Polym. Sci.*, **267**, 668 (1989).
14. P. Dobbert, *Acta Polym.*, **41**, 9 (1990).

Received March 16, 1992
Accepted June 3, 1993